The Influence of Microstructure on Nanomechanical and Diffusion Barrier Properties of Thin PECVD SiO$_X$ Films Deposited on Parylene C Substrates

David Framil[1], Matthias Van Gompel[2], Florian Bourgeois[2], Ivo Furno[3] and Yves Leterrier[1]*

[1] Laboratory for Processing of Advanced Composites (LPAC), Ecole Polytechnique Fédérale de Lausanne (EPFL), Lausanne, Switzerland, [2] Comelec SA, La Chaux-de-Fonds, Switzerland, [3] Swiss Plasma Center (SPC), Ecole Polytechnique Fédérale de Lausanne (EPFL), Lausanne, Switzerland

Plasma-enhanced chemical vapor deposition (PECVD) was used to deposit SiO$_X$ thin films of varying thicknesses on parylene C substrates, using hexamethyldisiloxane (HMDSO) as a precursor. The microstructure of SiO$_X$ coatings was analyzed using X-ray photoemission spectroscopy (XPS), nanoindentation, and spectroscopic ellipsometry. The composition ranged from oxygen-rich oxides with large silanol OH content to hybrid oxides with larger organic content, while refractive index varied from 1.45 to 1.5 depending on the specimen. Reduced moduli of coatings obtained by nanoindentation varied between 15 and 59 GPa and could be correlated with permeability to oxygen and water vapor through the existence of porosity in a broader sense. It can be concluded that the barrier properties are the result of a complex interplay of microstructural features, with porosity, silanol, and carbon content playing important roles in the final thin film properties.

Keywords: thin film, barrier, XPS, ellipsometry, nanoindentation, porosity

INTRODUCTION

Thin metal oxide films are extensively used as gas and water vapor diffusion barriers for polymer substrates in a variety of fields due to their interesting permeability range, transparency and dielectric properties, adaptability to industrial practice, and low relative costs. This includes applications in the food packaging industry (Dole et al., 2006; Duncan, 2011; Siracusa, 2012), selective drug delivery in biomedical applications (Fu and Kao, 2010; Kumari et al., 2010), and microelectronics encapsulation (Anderson et al., 1988; Birkelund et al., 2011). However, other applications such as encapsulation of organic light emitting diodes (OLED) put stringent requirements on permeability tolerance (Leterrier, 2003; Yu et al., 2016), generally many orders of magnitude below the usual values for polymers. Barrier properties of polymers can be improved to a certain extent by surface treatment (Arefi et al., 1992; Chu et al., 2002; Yoshida et al., 2013; Nemani et al., 2018), but coating the polymer with a low-permeability inorganic thin film remains a versatile approach, typically leading to one to two orders of magnitude improvement of the barrier, controlled by the process-induced defects in the film. The same coating processes also enable the fabrication of multilayer organic-inorganic structures, which allow for decoupling defects in the inorganic film, and improved barrier properties by up to six orders of magnitude (Bülow et al., 2014; Zhang et al., 2015; Lim et al., 2016). SiO$_X$ thin films have been widely used for this purpose

due to the wealth of deposition techniques available on a wide range of polymeric substrates, in particular plasma enhanced chemical vapor deposition (PECVD) (Inagaki et al., 2000, 2002; Lee et al., 2006; Schneider et al., 2009; Vasko et al., 2009; Liu et al., 2010; Lu et al., 2015; Jousseaume et al., 2017; Liao et al., 2018).

Focus of the present study is on parylene C, used as a passivation barrier in the medical device field due to its intrinsically low permeability, good dielectric properties, biocompatibility, and conformal deposition ability (Feili et al., 2005; Rizzi et al., 2013; Zeniieh et al., 2014; Golda-Cepa et al., 2015). The parylene substrates are deposited with a CVD-like process in a vacuum chamber. This equivalent deposition method compared to the PECVD used to form SiO$_x$ films makes it possible to deposit both the polymer and the oxide in the same vacuum chamber. SiO$_x$ thin films deposited on parylene C substrates using PECVD have proven valuable to date in order to further improve their barrier properties (Wuu et al., 2006; Potscavage et al., 2009; Hogg et al., 2014; Kim et al., 2014). PECVD from organosilane precursors may however lead to undesired organic contamination of the expected Si–O network and to a complex population of defects, and these two factors severely degrade the barrier performance (Roberts et al., 2002).

The objective of the work is to study whether a correlation between the permeability to gases and the Young's modulus of SiO$_x$ thin films can be established, based on microstructural information. Such a correlation would greatly facilitate the optimization of the PECVD process, and the characterization of the barrier properties of the films, which are both time consuming, using fast and automated nanoindentation analyses. To this end, we decided to produce three stoichiometries with higher carbon amounts to have a broader account on properties variability, and provide detailed investigations of the relations between the structure and composition of SiO$_x$ films and resulting mechanical properties and barrier to oxygen and water vapor. We confirm the strong influence of the film stoichiometry and establish a porosity-based model, which correlates the barrier to the mechanical properties of the films.

MATERIALS AND METHODS

Materials
Samples were produced in a hybrid reactor developed by Comelec (La Chaux-de-Fonds, Switzerland). This configuration allows sequential multilayer deposition of SiO$_x$/parylene dyads in a 30 liters chamber, without breaking the vacuum, thus avoiding surface contamination between layers. Parylene films with a thickness of 28 μm were deposited first using a standard Gorham process (Gorham, 2003) onto a glass substrate (7.5 × 5.25 cm) coated with a demolding agent. A venting step was added in order to introduce reference silicon wafers in the chamber for further characterization purposes. Subsequently, SiO$_x$ single layers of thicknesses ranging from 40 to 170 nm were deposited by means of PECVD on both parylene-coated glass substrates and silicon wafers, using hexamethyldisiloxane (HMDSO) as a SiO$_x$ precursor. Reactor configuration and parameters such as gas flows, plasma power, time, and pressure were varied in order to produce a set of 20 distinctly different samples.

X-Ray Photoelectron Spectroscopy (XPS)
The stoichiometry and composition of the SiO$_x$ films deposited on silicon were assessed using XPS. Measurements were performed in a PHI VersaProbe II scanning XPS microprobe (Physical Instruments AG, Germany) using a monochromatic Al K X-ray source of 45.7 W power with a beam size of 100 μm and an energy range up to 1,400 eV. The spherical capacitor analyzer was set at 45° take-off angle with respect to the sample surface, and the XPS beam was calibrated using adventitious carbon at 284.8 eV. The system includes a 2 kV argon ion beam to sputter layers of material of defined thickness, thus enabling a depth-dependent probing of the composition. The removal rate was set up to 9.2 nm/min as calibrated on SiO$_2$. The general SiO$_x$C$_y$ stoichiometry was obtained using a broad spectrum. The PHI Multipak software was used to calculate the area under the Si 2p, O 1s, and C 1s peaks, and the results were normalized with respect to the silicon value:

$$x = \frac{Area\,(O\,1s)}{Area\,(Si\,2p)}, \qquad (2.1)$$

$$y = \frac{Area(C\,1s)}{Area\,Si\,2p}. \qquad (2.2)$$

Narrow spectra (525–540 eV for O 1s, 94–110 eV for Si 2p, and 280–295 eV for C 1s) were also acquired to analyze the chemical composition and the occurrence of chemical shifts. OriginLab software was used to fit the spectra taken from the outermost surface region, other than the adventitious carbon first layer, by using asymmetric Voigt profiles (Jain et al., 2018). Single peak fit was used where possible to identify compound lines, yielding coefficients of correlation > 0.997 in most cases. Deconvolution of peaks and calculation of areas underneath was performed only as a qualitative verification of species present, or in cases where a single peak fit was not satisfactory. Due to limitations in access to equipment, only 16 samples out of 20 were characterized by XPS.

Ellipsometry
The optical properties of the SiO$_x$ films deposited on silicon were assessed using spectroscopic ellipsometry. Measurements were performed using a Semilab SE-2000 ellipsometer equipped with software-controlled polarizer and analyzer arms, which provides a spectral range from 190 nm to 25 μm. Three measurements at 10 different incident angles ranging from 65° to 75° were taken at distinctly different spots of the surface, adding up to 30 measurements per sample. Experimental Ψ and Δ curves were fitted to a three-layer model (Tompkins and Irene, 2005), comprising an ambient layer of known properties [refractive index of air (632.8 nm) = 1.00152], a SiO$_x$ layer of properties to determine, and a silicon substrate layer of known properties [refractive index n_{Si}(632.8 nm) = 3.8811, extinction index k_{Si} (632.8 nm) = 0.0195]. Due to the expected transparent nature of the SiO$_x$ film and its wavelength dependence, a Cauchy-type model was used to extract the optical properties:

$$n\,(\lambda) = n_{inf} + \frac{B}{\lambda^2}, \qquad (2.3)$$

With n_{inf} being the low-energy refractive index, B the first coefficient of the Cauchy model and λ the wavelength. The model was used only in the 1–4.5 eV range because of the large influence of depolarization effects in Ψ and Δ at higher energies. The values of the fitted parameters and B were calculated with the Spectroscopic Ellipsometry Analyzer (SEA) software provided by Semilab, using a non-linear least-squares approach based on a QR decomposition Levenberg-Marquardt algorithm with a tolerance of 10^{-6}. The coefficients of determination were $R^2 > 0.997$ in any case, while the average root mean squared error for all the samples was equal to 0.615.

Oxygen and Water Vapor Transmission Rates

The oxygen (OTR) and water vapor (WVTR) transmission rates of the SiO$_x$ coated parylene films were measured using dedicated Systech Illinois analyzers. The testing system consists in both cases of two chambers with watertight upper and lower compartments separated by the film to be tested. The diffusing species, either dry or wet, are injected at a flow of 20 sccm in the top chamber, while a carrier gas, namely nitrogen, is blown at 10 sccm in the lower chamber. OTR and WVTR values are calibrated beforehand using a thin film of PET with known properties at specific temperature and humidity conditions. The background baselines used during testing were 0.5 ppm for oxygen and 4 ppm for water vapor. OTR experiments were carried out in a Systech 8001 at a temperature of 38°C and 90% relative humidity, for an oxygen partial pressure gradient ΔPO_2 of 1 atm. On the other hand, WVTR tests were carried out in a Systech 7001 at a temperature of 38°C and 50% relative humidity, for a calculated water vapor partial pressure gradient ΔP_{H_2O} of 3.33×10^{-2} bar according to Buck equations (Buck, 1981). The films to be tested were cut to approximate sizes of 3×3 cm using a scalpel and further detached from the glass substrates. They were then sandwiched between two metal masks with circular apertures of 5 cm^2 using high pressure lube and polymer joints. The full mask was introduced in the testing chamber and mounted using high pressure lube, and the system was left to evolve with time to enable the diffusing species to permeate the film. The transmission rate, related to the amount of diffusing species detected by the sensors in the lower compartments (g/m^{2}day for WVTR and cm^3/m^{2}day for OTR), was recorded when a steady state was reached, and further averaged for the two chambers. Due to the different nature of the samples, the time to reach the steady state could range from 3 h to several days. The experimental detection limit was 0.008 (cm^3 mm)/(m^2 day atm) for oxygen and 0.02 (g mm)/(m^2 day bar) for water vapor.

As a first approximation, oxygen, and water vapor permeabilities for SiO$_x$ were calculated using laminate theory (Roberts et al., 2002):

$$\frac{\Delta P_{O_2}}{OTR} = \frac{d_{SiO_x,O_2}}{P_{SiO_x,O_2}} + \frac{d_{ParC,O_2}}{P_{ParC,O_2}}, \quad (2.4)$$

$$\frac{\Delta P_{H_2O}}{WVTR} = \frac{d_{SiO_x,H_2O}}{P_{SiO_x,H_2O}} + \frac{d_{ParC,H_2O}}{P_{ParC,H_2O}}. \quad (2.5)$$

Where P_{SiO_x} is the permeability of SiO$_x$, and d_{SiO_x} and d_{ParC} are, respectively, the thicknesses of the SiO$_x$ film and the parylene C substrate. The permeability of parylene C was measured independently, and values of 3.8 (cm^3 mm)/(m^2 day atm) and 0.625 (g mm)/(m^2 day bar) were found for oxygen and water vapor, respectively.

Nanoindentation

Nanoindentation of SiO$_x$ films deposited on silicon was carried out in a Hysitron TriboIndenter TI95 with a Berkovich tip and displacement-controlled feedback at different depths. The tip contact area was calibrated using a fused quartz sample, and the reduced Young's modulus (E_r) was extracted using the Oliver & Pharr method (Oliver and Pharr, 1992) using the acquisition software, rather than the Young's modulus since the Poisson's ratio of the investigated films was unknown. Data outliers, defined as any point for which its difference with the average is larger than three times the standard deviation, were removed from the analysis. A fixed displacement rate of 1 nm/s was used for loading and unloading, and a 5 s interval at maximum target depth was kept to ensure a comparatively fast enough unloading rate in order to minimize the effect of any type of relaxation in the extraction of the mechanical properties (Hochstetter et al., 2007). According to the combination of mechanical properties of the SiO$_x$ film and the Si substrate, a probing depth of 10% or less would remain a safe choice to determine the thin film elastic moduli (Gamonpilas and Busso, 2004). However, this would mean staying below 2 nm indentation depth for some of the coatings, and potentially increasing the sources of error due to local roughness, tip rounding, or area calibration (Menčík, 2012; Jakes, 2018). To avoid this uncertainty, the subsurface mechanical properties were mapped using a grid consisting of 15 indents designed to ramp from 5 nm maximum displacement to 50 nm. The horizontal separation between indents was kept at 15 μm to avoid interference between developed plastic zones, and the grid was run 10 times in total on different areas to obtain statistically significant values. Indentation areas were selected to be as flat and free of roughness as possible.

In this testing configuration the substrate effect needs to be taken into account, and therefore the coating elastic modulus was extracted by fitting the composite reduced modulus E_r as a function of indentation contact depth, d. For better accuracy, the reduced modulus of the substrate $E_{r,s}$ was considered an unknown parameter (Antunes et al., 2007) in addition to the reduced modulus of the coating $E_{r,c}$ and the fitting parameter α. The three parameters were extracted using a non-linear optimization based on a trust region reflective algorithm (Branch et al., 1999) with an absolute error cost function provided by the *scipy.optimize* package in Python. The final model was selected based on the minimum deviation of the fitted substrate modulus with respect to the experimental value, which ranged between 134.5 and 145.9 GPa depending on the type of silicon. Finally, the majority of the samples could be fitted using an inverse Doerner-Nix relationship (Equation 2.6) or an inverse exponential
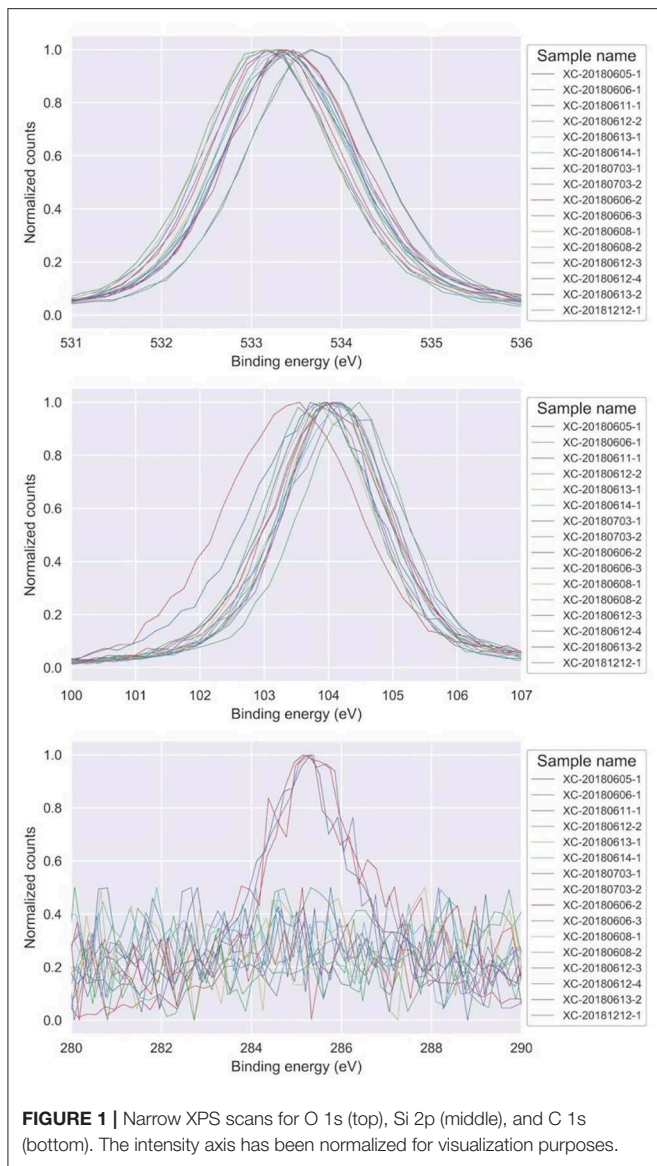
FIGURE 1 | Narrow XPS scans for O 1s (top), Si 2p (middle), and C 1s (bottom). The intensity axis has been normalized for visualization purposes.

(Equation 2.7) (Antunes et al., 2007):

$$E_r = E_{r,f}\left(1 - e^{-\alpha\frac{d_{SiO_x}}{h}}\right) + E_{r,s}e^{-\alpha\frac{d_{SiO_x}}{h}}, \quad (2.6)$$

$$\frac{1}{E_r} = \frac{1}{E_{r,s}}\left(1 - e^{-\alpha\frac{h}{d_{SiO_x}}}\right) + \frac{1}{E_{r,f}}e^{-\alpha\frac{h}{d_{SiO_x}}}. \quad (2.7)$$

RESULTS

Composition and Optical Properties

Samples were classified into three main categories based on stoichiometry according to the XPS results. The survey spectra can be found in **Figure S1**. Firstly, oxygen-rich silicon oxide with formula SiO$_{2.16-2.24}$, virtually carbon-free (under equipment detection limit). Secondly, stoichiometric SiO$_2$ with low carbon
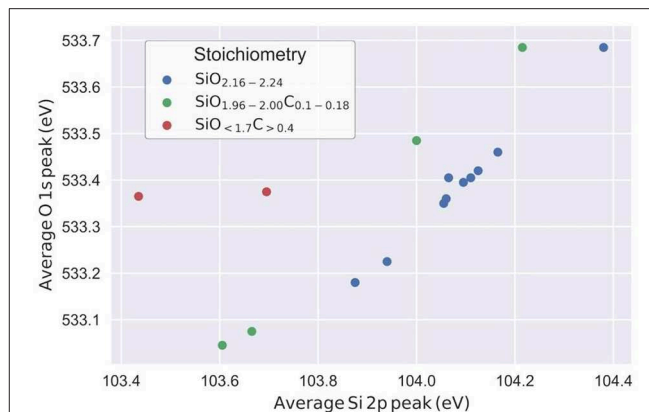

FIGURE 2 | Average O 1s peak energy as a function of average Si 2p peak energy.
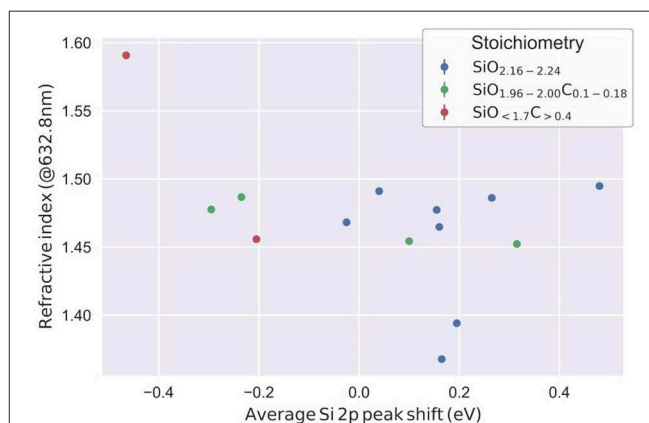
FIGURE 3 | Refractive index of the SiO$_x$ films as a function of average Si 2p peak shift.

content and general formula SiO$_{1.96-2}$C$_{0.1-0.18}$. And thirdly, oxides with lower oxygen and higher carbon content, with a SiO$_{<1.7}$C$_{>0.4}$ stoichiometry. As shown in **Figure 1**, narrow peaks were present between ranges of 533–533.7 eV for O 1s, 103.4–104.4 eV for Si 2p, and 284.2–285.7 eV for C 1s. Individual fitting of all Si2p peaks can be also found in **Figure S2**. **Figure 2** depicts the average energy for the O 1s peaks as a function of the energy of the Si 2p peaks. Two subgroups can be identified: one comprising all the oxygen rich oxides plus two low energy peak low carbon oxides, and the other comprising the four remaining outliers (two high carbon oxides plus two high energy peak low carbon oxides). A linear trend is clearly visible for all the oxygen-rich oxides. The carbon-containing oxides are grouped based on the energy of the main C 1s peak, which corresponds to 284.8 eV for the two low energy low carbon oxides, and to 285.4 eV for the others.

Independently of stoichiometry, the refractive index n of the SiO$_x$ films at 632.8 nm was found to fall within a range of 1.45–1.5, except for two clear outliers. All films were completely transparent, with an extinction coefficient of exactly zero. **Figure 3** shows the refractive index as a function of average Si 2p peak shift, defined as the difference in binding energy between the experimental peak and the expected peak of thermal SiO$_2$, located
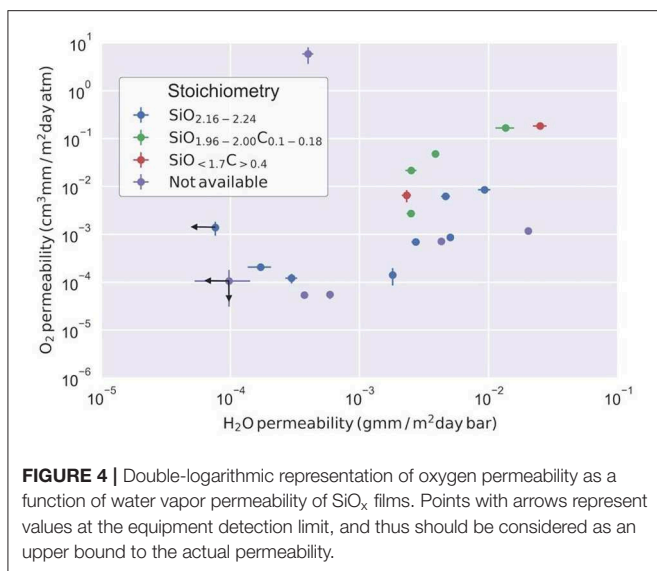
FIGURE 4 | Double-logarithmic representation of oxygen permeability as a function of water vapor permeability of SiO$_x$ films. Points with arrows represent values at the equipment detection limit, and thus should be considered as an upper bound to the actual permeability.

FIGURE 5 | Composite reduced modulus E$_r$ as a function of contact depth d normalized by the thin film thickness d$_{SiOx}$. The reduced modulus of the coating E$_{r,f}$ is the extrapolation to $d = 0$ using the inverse exponential model. Black lines indicate the Young's modulus of fused silica (69.7 GPa) and silicon (~145 GPa).

at around 103.9 eV (Montero et al., 1990; Alfonsetti et al., 1994). For oxygen-rich oxides other than the outliers below 1.4, a weak positive increase of n with the shift can be observed. Low carbon oxides show an opposite negative trend, while high carbon oxides are always shifted to lower binding energies.

Oxygen and Water Vapor Permeability

An increasing correlation that spans up to three orders of magnitude can be observed in **Figure 4** for the intrinsic permeability to oxygen and water vapor of the SiO$_x$ films. The behavior seems to be independent on the specific stoichiometry as each composition group spans at least two orders of magnitude in oxygen permeability and one order in water vapor permeability. On average, carbon-containing oxides show higher permeabilities than oxygen-rich oxides.
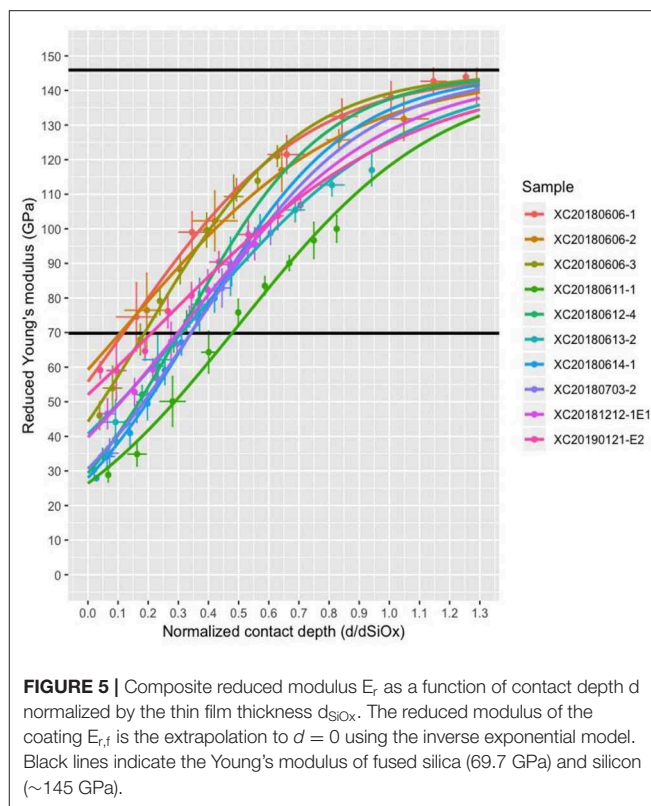
Elastic Modulus

Examples of load-displacement curves are shown in the **Supplementary Material**. The extraction of SiOx reduced modulus for the inverse exponential model (Equation 2.7) is shown in **Figure 5**. Obtained elastic moduli for all samples vary from 15 to 59 GPa, values that are consistently below the expected value of 69.7 GPa for fused quartz (Oliver and Pharr, 1992).

A negative correlation between reduced modulus and permeability, both to oxygen and water vapor, is also evident in **Figure 6**. This relationship seems to be independent of the stoichiometry considered over at least two orders of magnitude, although carbon-containing oxides show systematically lower reduced moduli.

POROSITY-BASED MODEL

It is well-known that the density of SiO$_x$ thin films changes depending on the process parameters (Pan et al., 1985; Vianna et al., 2001). Additionally, the variation in effective Young's modulus E for a given ceramic composition can be explained in terms of porosity (Kovacik, 1999; Roberts and Garboczi, 2000; Jang and Matsubara, 2005; Pabst et al., 2006) through a general Phani-Niyogi relation (Equation 4.1), and permeability P in nanoporous glasses can be described by means of Knudsen diffusion (Shelekhin et al., 1995; Roberts et al., 2002), which in turn also depends on porosity (Equation 4.2):
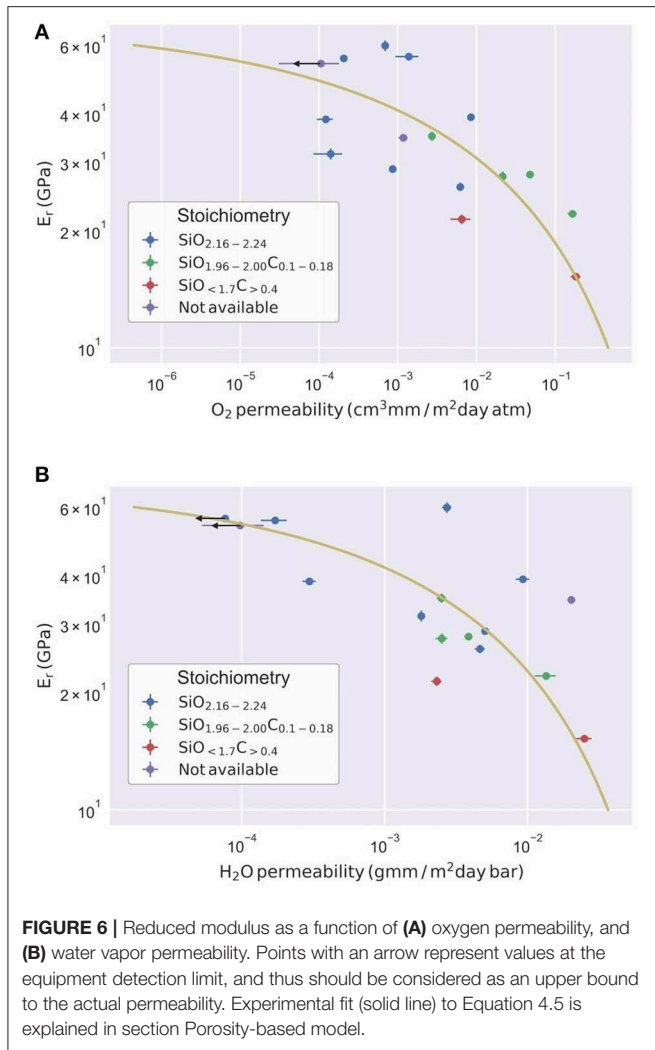
$$E = E_0 \left(1 - \frac{\phi}{\phi_c}\right)^{[E]\phi_c}, \qquad (4.1)$$

$$P = D_p \sqrt{\frac{8}{\pi MRT}} \frac{\phi}{3\tau} e^{-\frac{\Delta E}{RT}} . \qquad (4.2)$$

The effective Young's modulus E depends on the porosity ϕ, the Young's modulus of the dense material E_0, a percolation threshold ϕ_c, and an intrinsic elastic modulus $[E]$. On the other hand, the permeability P is influenced by the pore diameter D_p, the molecular weight of the diffusing species M, the temperature T, the ideal gas constant R, the tortuosity τ, and an Arrhenius term with an activation energy ΔE. Considering the fact that experiments were carried out at the same temperature for oxygen and water vapor, Equation 4.2 can be rewritten using a constant A as follows:

$$P = AD_p \frac{\phi}{\tau}. \qquad (4.3)$$

Different porosity-tortuosity relations have been proposed in the literature (Matyka et al., 2008), either found experimentally or derived through theoretical considerations. On the other

FIGURE 6 | Reduced modulus as a function of **(A)** oxygen permeability, and **(B)** water vapor permeability. Points with an arrow represent values at the equipment detection limit, and thus should be considered as an upper bound to the actual permeability. Experimental fit (solid line) to Equation 4.5 is explained in section Porosity-based model.

FIGURE 7 | Average porosity calculated for the whole sample set using Equations 4.1 and 4.4.

TABLE 1 | Fitting parameters for oxygen and water vapor permeation.

Gas	[E]	ϕ_c	A	β
Oxygen	1.81	0.96	8.48	6.62
Water vapor	~ 1.90	~ 1.00	0.18	3.58

Parameter A has permeability units as defined in section Oxygen and water vapor transmission rates.

DISCUSSION

Composition and Optical Properties

XPS studies reveal that SiO$_x$ can be considered to be a combination of different oxides in which silicon displays different oxidation states (Bell and Ley, 1988; Finster et al., 1990; Alfonsetti et al., 1993, 1994; Vasquez et al., 2002; Clergereaux et al., 2007). This explanation is especially suited for oxygen deficient oxides, as the occurrence of lower oxidation states can be linked to a shift of the Si 2p peak to lower energies. However, oxygen-rich oxides (SiO$_{2.16-2.24}$) show a shift to higher energies, up to ~0.5 eV with respect to the thermal oxide. This behavior can be explained in terms of hydroxyl groups bonded to silicon atoms (Montero et al., 1990; Paparazzo et al., 2002), and therefore yielding partially hydroxylated oxides. This effect has also been observed by FTIR on SiO$_x$ thin films deposited using TEOS as a precursor (Jeong et al., 2002) and in plasma-polymerization of siloxanes (De Geyter et al., 2009).

Low carbon oxides (SiO$_{1.96-2}$C$_{0.1-0.18}$) show two distinct behaviors. On the one hand, the specimens with the Si and O peaks shifted to lower energies show a carbon peak at around 284.8 eV, indicating that carbon is chemically bonded to silicon. Based on the nature of the HMDSO precursor the compound is likely to be polydimethylsiloxane (PDMS) (Morra et al., 1990; Webster et al., 2005), and these specimens can be considered as a type of organic-inorganic hybrid with general formula
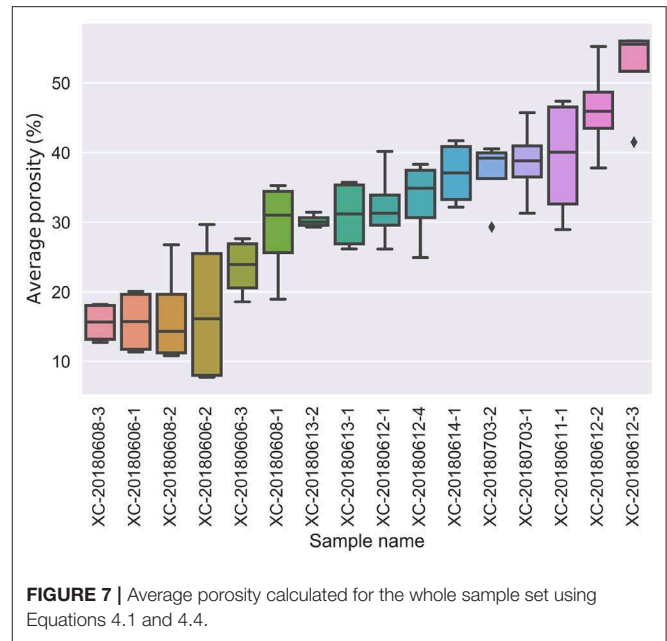
hand, empirical power relations have also been found between pore radius, permeability and porosity in the context of gas permeation through tight porous media (Ziarani and Aguilera, 2012). Taking this into consideration, permeability can be rewritten as a power law with a β exponent:

$$P = A\varphi^\beta . \qquad (4.4)$$

and therefore the effective Young's modulus can be linked to permeability combining Equations 4.1 and 4.5 as follows:

$$P = A \left[\phi_c \left(1 - \left(\frac{E}{E_0}\right)^{\frac{1}{[E]\phi_c}} \right) \right]^\beta . \qquad (4.5)$$

The fit of reduced modulus and permeability using Equation 4.5 is shown in **Figure 7**, using the same algorithm optimization as described in section Nanoindentation for nanoindentation analysis. The fitting parameters are summarized in **Table 1**.

(SiO$_{2.05-2.08}$) (SiOC$_2$)$_{0.05-0.08}$. On the other hand, specimens with Si peaks shifted to higher energies display a much sharper shift in the O peak together with a C peak at around 284.8 eV. This is a signature of chemical bonding between oxygen and carbon, and therefore the formation of an organic compound inside a larger SiO$_x$ matrix. According to the nature of the precursor and the C 1s and O 1s peak energies it is reasonable to suggest that this element is a type of polymethylmethacrylate (PMMA) (Moulder et al., 2002), with a general stoichiometry of SiO$_{1.88-1.92}$(C$_5$O$_2$H$_8$)$_{0.032-0.036}$. From this analysis, it is evident that specimens with a very similar stoichiometry can be structurally different.

Finally, the two higher carbon containing samples are also structurally different. One of them forms a PMMA-like organic compound in a SiO$_x$ matrix, resulting in a general stoichiometry of SiO$_{1.56}$ (C$_5$O$_2$H$_8$)$_{0.08}$. The other forms silicon and oxygen-based organic compounds simultaneously. In this latter case, the Si 2p peak can be clearly deconvoluted into two lines centered at 102.7 and 104.5 eV, with a relative area ratio of. This yields a general formula of SiO$_{0.91}$(SiOC$_2$)$_{0.6}$(C$_5$O$_2$H$_8$)$_{0.27}$, indicative of a very oxygen-deficient SiO$_x$ matrix hosting regions of PDMS- and PMMA-like compounds. The observed refractive index range between 1.45 and 1.5 can be explained in light of these prior considerations. It has to be noted that the refractive index is always larger for the carbon-free oxygen-rich oxides than the refractive index of fused silica, which is 1.457 (Malitson, 2008), meaning that the result of hydroxylation of silicon is an increase in refractive index. While it is well-known that oxygen-deficient SiO$_x$ has a higher refractive index due to an increase in metallicity (Miyazaki, 2010), nothing has been found in the literature for the oxygen-rich case.

Apart from this hypothesis, it has to be considered that this type of films tends to be hydrated (Blanchard et al., 2015), and if the carbon-containing oxides are also taken into account, this would imply that the microstructure is very likely to incorporate several phases with different optical properties. The related refractive indices would be >1.5 (oxygen-deficient SiO$_x$), 1.5 (hydroxylated SiO$_2$), 1.49 (PMMA) (Beadie et al., 2015), 1.457 (SiO$_2$), 1.4 (PDMS) (Lee et al., 2008), 1.33 (water), and 1.0 (air), and the effective refractive index would be the outcome of a combination of them.

Permeability

It is well-established that permeability depends on SiO$_x$ film thickness, as very thin layers do not ensure maximum coverage and thicker layers can develop microcracks which in turn increase the permeability (Chatham, 1996; Sobrinho et al., 2000; Roberts et al., 2002; Leterrier, 2003). The range of thicknesses used in our experiments is between these two limit cases, and therefore the permeabilities calculated using laminate theory can be considered to be a representative property of the material. In light of this composition analysis, the trend observed in **Figure 4** is the expected one, with oxygen-rich oxides showing overall lower permeabilities than carbon-containing ones (Markov et al., 2014; Lu et al., 2015). However, the organic content by itself does not explain the permeability ranges observed, as carbon-containing oxides overlap with carbon-free oxides. Furthermore,

the latter shows a spread of two orders of magnitude in both oxygen and water vapor permeability which cannot be correlated with the Si 2p peak shift of hydroxylated oxides, therefore suggesting a major influence of nanoporosity in the barrier properties. The type and fraction of organic phases do not justify the permeabilities observed for carbon-containing oxides, also suggesting a large influence of nanoporosity also in the hybrid oxides. The data from **Table 1** was used to calculate the porosities for the whole set of samples, resulting in a range of porosities between 10 and 50% as shown in **Figure 7**.

Based on these considerations it is very likely that SiO$_x$ thin films display some type of nanoporosity in the 0.29–0.55 nm pore size range (Ito et al., 2007), making Knudsen diffusion the main permeation mechanism (Kirchheim et al., 2017). This is also supported by the fact that all the experiments were carried out at the same temperature, yet the results for similar stoichiometry can be quite different. Furthermore, Knudsen diffusion is influenced by the type of diffusing molecule since it depends on collisions between molecules and pore walls. This is captured by the power law dependence on porosity suggested in Equation 4.4. The relation also highlights the importance of tortuosity in the diffusion mechanism, as the experimental results (**Figure 4**) reveal a slope different from the expected unity value if tortuosity were considered constant.

Nanomechanical Properties

Nanomechanical characterization of SiO$_x$ thin films deposited by PECVD tends to rely on hardness assessment or in testing SiO$_2$-like coatings (Benitez et al., 2000; Cao and Zhang, 2008; Subhash et al., 2010; Albuquerque et al., 2014), with SiO$_2$ values reported in the literature ranging from 24 to 120 GPa. However, a direct comparison might not be feasible due to the lack of information regarding composition of the deposited coatings, questionable extraction of mechanical properties (substrate effect not considered, for instance where reported values exceed 75 GPa), testing of complex structures where experiment design and interpretation of mechanical properties is far from being trivial, or all of these simultaneously (Cabibbo et al., 2013; Polyakov et al., 2014; Reddy et al., 2014). On the other hand, molecular simulations of SiO$_2$ thin films and experimental work are in good agreement with the typical fused silica values (Kim and Kim, 2013; Chen et al., 2018), which are consistently higher than the values obtained in this work. Recently, nanomechanical properties of hybrid DLC-SiO$_x$ nanocomposites have shown a remarkable range of elastic properties achievable depending on deposition process parameters (Grenadyorov et al., 2018). However, to the best of our knowledge, there is no work that addresses nanomechanical properties of SiO$_x$ thin films from a structural point of view.

According to the prior discussion, the existence of nanoporosity would be a major influence to explain the experimental variation in elastic moduli. Furthermore, the fit to the Phani-Niyogi relation yields a percolation threshold of $\phi \approx 1$ and an intrinsic elastic modulus of $[E] = 1.8–1.9$. This latter value is in good agreement with the theoretical values for a material such as SiO$_2$ with a Poisson's ratio of 0.17 (Pabst et al., 2006). The mechanical behavior could then be reduced to

a simple Coble-Kingery relation where $[E] = 2.0$ and $\phi_c \equiv 1$, which points out to the existence of spherical not-interconnected pores in the SiO$_x$ thin films. On the other hand, the existence of an organic phase also influences the mechanical properties, as polymer-like materials have systematically lower elastic moduli (Hochstetter et al., 2007).

As a matter of fact, the nanoindentaiton tests are much faster than the permeability tests. A practical implication of the proposed approach is thus to provide a strategy for fast assessment of the barrier performance of thin films on polymers, relying on the mechanical analysis of the films.

CONCLUSIONS

SiO$_x$ thin films of thicknesses in the range from 40 to 170 nm were deposited by PECVD on parylene C and silicon substrates, using HMDSO as a precursor. Different stoichiometries ranging from SiO$_{<1.7}$C$_{>0.4}$ to SiO$_{2.16-2.24}$ were found by XPS, and the nature of the microstructure consisted of a main SiO$_2$ host containing fractions of silanols, pores, or carbonaceous compounds. This was confirmed by refractive index values from 1.45 to 1.5. The main result from the present study is that it is the porosity, more than the stoichiometry, which controls the properties. The Young's modulus derived from nanoindentation experiments varied between 15 and 59 GPa and could be correlated with permeability to oxygen and water vapor through a major influence of porosity. A Coble-Kingery relation arose from this correlation, suggesting that pores are spherical in shape, and a quantification of porosity showed a range between 0.1 and 0.5 for the samples tested. Despite the heterogeneous microstructure of the specimens, it was found that elastic modulus is a good indicator of barrier performance for SiO$_x$/parylene C combinations.

DATA AVAILABILITY STATEMENT

The datasets generated for this study are available on request to the corresponding author.

AUTHOR CONTRIBUTIONS

DF and MV performed the work and wrote the paper. FB, IF, and YL designed the investigation, planned the production of the samples, and wrote parts of the paper.

FUNDING

ACKNOWLEDGMENTS

SUPPLEMENTARY MATERIAL

The Supplementary Material for this article can be found online at: https://www.frontiersin.org/articles/10.3389/fmats.2019.00319/full#supplementary-material

REFERENCES

Albuquerque, M. D., Santos, E., Perdone, R. R., and Simao, R. A. (2014). Effect of self-bias voltage on the wettability, chemical functionality and nanomechanical properties of hexamethyldisiloxane films. *Thin Solid Films* 564, 73–78. doi: 10.1016/j.tsf.2014.05.012

Alfonsetti, R., De Simone, G., Lozzi, L., Passacantando, M., Picozzi, P., and Santucci, S. (1994). SiO$_x$ surface stoichiometry by XPS: a comparison of various methods. *Surf. Interface Anal.* 22, 89–92. doi: 10.1002/sia.740220122

Alfonsetti, R., Lozzi, L., Passacantando, M., Picozzi, P., and Santucci, S. (1993). XPS studies on SiO$_x$ thin films. *Appl. Surf. Sci.* 70, 222–225. doi: 10.1016/0169-4332(93)90431-A

Anderson, J. E., Markovac, V., and Troyk, P. R. (1988). Polymer encapsulants for microelectronics: mechanisms for protection and failure. *IEEE Trans. Components Hybrids Manuf. Technol.* 11, 152–158. doi: 10.1109/33.2979

Antunes, J. M., Fernandes, J. V., Sakharova, N. A., Oliveira, M. C., and Menezes, L. F. (2007). On the determination of the Young's modulus of thin films using indentation tests. *Int. J. Solids Struct.* 44, 8313–8334. doi: 10.1016/j.ijsolstr.2007.06.015

Arefi, F., Andre, V., Montazer-Rahmati, P., and Amouroux, J. (1992). Plasma polymerization and surface treatment of polymers. *Pure Appl. Chem.* 64, 715–723. doi: 10.1351/pac199264050715

Beadie, G., Brindza, M., Flynn, R. A., Rosenberg, A., and Shirk, J. S. (2015). Refractive index measurements of poly(methyl methacrylate) (PMMA) from 0.4–1.6 μm. *Appl. Opt.* 54, 139–143. doi: 10.1364/AO.54.00F139

Bell, F. G., and Ley, L. (1988). Photoemission study of SiO$_x$ (0<x<2) alloys. *Phys. Rev. B* 37, 8383–8393. doi: 10.1103/PhysRevB.37.8383

Benitez, F., Martinez, E., and Esteve, J. (2000). Improvement of hardness in plasma polymerized hexamethyldisiloxane coatings by silica-like surface modification. *Thin Solid Films* 377–378, 109–114. doi: 10.1016/S0040-6090(00)01393-6

Birkelund, K., Nørgaard, L., and Thomsen, E. V. (2011). Enhanced polymeric encapsulation for MEMS based multi sensors for fisheries research. *Sens. Actuators A Phys.* 170, 196–201. doi: 10.1016/j.sna.2011.06.008

Blanchard, N. E., Naik, V. V., Geue, T., Kahle, O., Hegemann, D., and Heuberger, M. (2015). Response of plasma-polymerized hexamethyldisiloxane films to aqueous environments. *Langmuir* 31, 12944–12953. doi: 10.1021/acs.langmuir.5b03010

Branch, M. A., Coleman, T., and Li, Y. (1999). A subspace, interior, and conjugate gradient method for large-scale bound-constrained minimization problems. *SIAM J. Sci. Comput.* 21, 1–23. doi: 10.1137/S1064827595289108

Buck, A. L. (1981). New equation for computing vapor pressure and enhancement factor. *J. Appl. Meteorol.* 20, 1527–1532. doi: 10.1175/1520-0450(1981)020<1527:NEFCVP>2.0.CO;2

Bülow, T., Gargouri, H., Siebert, M., Rudolph, R., Johannes, H. H., and Kowalsky, W. (2014). Moisture barrier properties of thin organic-inorganic multilayers prepared by plasma-enhanced ALD and CVD in one reactor. *Nanoscale Res. Lett.* 9:223. doi: 10.1186/1556-276X.-9-223

Cabibbo, M., Ciccarelli, D., and Spigarelli, S. (2013). Nanoindentation hardness measurement in piling up SiO$_2$ coating. *Phys. Proc.* 40, 100–112. doi: 10.1016/j.phpro.2012.12.014

Cao, Z., and Zhang, X. (2008). Nanoindentation stress-strain curves of plasma-enhanced chemical vapor deposited silicon oxide thin films. *Thin Solid Films* 516, 1941–1951. doi: 10.1016/j.tsf.2007.09.033

Chatham, H. (1996). Oxygen diffusion barrier properties of transparent oxide coatings on polymeric substrates. *Surf. Coat. Technol.* 78, 1–9. doi: 10.1016/0257-8972(95)02420-4

Chen, J., Shi, J., Wang, Y., Sun, J., Han, J., Sun, K., et al. (2018). Nanoindentation and deformation behaviors of silicon covered with amorphous SiO$_2$: a molecular dynamic study. *RSC Adv.* 8, 12579–12607. doi: 10.1039/C7RA13638B

Chu, P. K., Chen, J. Y., Wang, L. P., and Huang, N. (2002). Plasma-surface modification of biomaterials. *Mater. Sci. Eng. R Rep.* 36, 143–206. doi: 10.1016/S0927-796X(02)00004-9

Clergereaux, R., Calafat, M., Benitez, F., Escaich, D., Savin de Larclause, I., Raynaud, P., et al. (2007). Comparison between continuous and microwave oxygen plasma post-treatment on organosilicon plasma deposited layers: effects on structure and properties. *Thin Solid Films* 515, 3452–3460. doi: 10.1016/j.tsf.2006.10.076

De Geyter, N., Leys, C., Morent, R., Van Vlierberghe, S., Dubruel, P., and Schacht, E. (2009). Plasma polymerisation of siloxanes at atmospheric pressure. *Surf. Eng.* 27, 627–633. doi: 10.1179/174329409X433858

Dole, P., Hankemeier, T., Cruz, C. D. L., Aucejo, S., Saillard, P., Feigenbaum, A. E., et al. (2006). Typical diffusion behaviour in packaging polymers application to functional barriers. *Food Addit. Contam.* 23, 202–211. doi: 10.1080/02652030500373661

Duncan, T. V. (2011). Applications of nanotechnology in food packaging and food safety: barrier materials, antimicrobials and sensors. *J. Colloid Interface Sci.* 363, 1–24. doi: 10.1016/j.jcis.2011.07.017

Feili, D., Schuettler, M., Doerge, T., Kammer, S., and Stieglitz, T. (2005). Encapsulation of organic field effect transistors for flexible biomedical microimplants. *Sens. Actuators A Phys.* 120, 101–109. doi: 10.1016/j.sna.2004.11.021

Finster, J., Klinkenberg, E. D., Heeg, J., and Braun, W. (1990). ESCA and SEXAFS investigations of insulating materials for ULSI microelectronics. *Vacuum* 41, 1586–1589. doi: 10.1016/0042-207X(90)94025-L

Fu, Y., and Kao, W. J. (2010). Drug release kinetics and transport mechanisms of nondegradable and degradable polymeric delivery systems. *Expert Opin. Drug Deliv.* 7, 429–444. doi: 10.1517/17425241003602259

Gamonpilas, C., and Busso, E. P. (2004). On the effect of substrate properties on the indentation behaviour of coated systems. *Mater. Sci. Eng. A* 380, 52–61. doi: 10.1016/j.msea.2004.04.038

Golda-Cepa, M., Brzychczy-Wloch, M., Engvall, K., Aminlashgari, N., Hakkarainen, M., and Kotarba, A. (2015). Microbiological investigations of oxygen plasma treated parylene C surfaces for metal implant coating. *Mater. Sci. Eng. C* 52, 273–281. doi: 10.1016/j.msec.2015.03.060

Gorham, W. F. (2003). A New. General synthetic method for the preparation of linear poly-p-xylylenes. *J. Polym. Sci. Part A 1 Polym. Chem.* 4, 3027–3039. doi: 10.1002/pol.1966.150041209

Grenadyorov, A. S., Solovyev, A. A., Oskomov, K. V., and Sypchenko, V. S. (2018). Influence of deposition conditions on mechanical properties of a-C:H:SiO$_x$ films prepared by plasma-assisted chemical vapor deposition method. *Surf. Coat. Technol.* 349, 547–555. doi: 10.1016/j.surfcoat.2018.06.019

Hochstetter, G., Jimenez, A., and Loubet, J. L. (2007). Strain-rate effects on hardness of glassy polymers in the nanoscale range. Comparison between quasi-static and continuous stiffness measurements. *J. Macromol. Sci. Part B* 38, 681–692. doi: 10.1080/00222349908248131

Hogg, A., Uhl, S., Feuvrier, F., Girardet, Y., Graf, B., Aellen, T., et al. (2014). Protective multilayer packaging for long-term implantable medical devices. *Surf. Coat. Technol.* 255, 124–129. doi: 10.1016/j.surfcoat.2014.02.070

Inagaki, N., Tasaka, S., and Hiramatsu, H. (2002). Preparation of oxygen gas barrier poly(ethylene terephthalate) films by deposition of silicon oxide films plasmapolymerized from a mixture of tetramethoxysilane and oxygen. *J. Appl. Polym. Sci.* 71, 2091–2100. doi: 10.1002/(SICI)1097-4628(19990321)71:12<2091::AID-APP20>3.0.C. O;2-A

Inagaki, N., Tasaka, S., and Nakajima, T. (2000). Preparation of oxygen gas barrier polypropylene films by deposition of SiO$_x$ films plasma-polymerized from mixture of tetramethoxysilane and oxygen. *J. Appl. Polym. Sci.* 78, 2389–2397. doi: 10.1002/1097-4628(20001220)78:13<2389::AID-APP160>3.0.CO;2-J

Ito, K., Oka, T., Kobayashi, Y., Suzuki, R., and Ohdaira, T. (2007). Variable-energy positron annihilation study of subnanopores in SiOCH-based PECVD films. *Radiat. Phys. Chem.* 76, 213–216. doi: 10.1016/j.radphyschem.2006.03.038

Jain, V., Biesinger, M. C., and Linford, M. R. (2018). The Gaussian-Lorentzian sum, product, and convolution (voigt) functions in the context of peak fitting Xray photoelectron spectroscopy (XPS) narrow scans. *Appl. Surf. Sci.* 447, 548–553. doi: 10.1016/j.apsusc.2018.03.190

Jakes, J. E. (2018). Improved methods for nanoindentation Berkovich probe calibrations using fused silica. *J. Mater. Sci.* 53, 4814–4827. doi: 10.1007/s10853-017-1922-8

Jang, B., and Matsubara, H. (2005). Influence of porosity on hardness and Young's modulus of nanoporous EB-PVD TBCs by nanoindentation. *Mater. Lett.* 59, 3462–3466. doi: 10.1016/j.matlet.2005.06.014

Jeong, J. Y., Tu, V. J., Selwyn, G. S., Hicks, R. F., Babayan, S. E., and Park, J. (2002). Deposition of silicon dioxide films with an atmospheric-pressure plasma jet. *Plasma Sour. Sci. Technol.* 7, 286–288. doi: 10.1088/0963-0252/7/3/006

Jousseaume, V., El Sabahy, J., Yeromonahos, C., Castellan, G., Bouamrani, A., and Ricoul, F. (2017). SiOCH thin films deposited by chemical vapor deposition: from low-κ to chemical and biochemical sensors. *Microelectron. Eng.* 167, 69–79. doi: 10.1016/j.mee.2016.10.003

Kim, H. J., and Kim, D. E. (2013). Effects of proximity on hardness and elastic modulus measurements of SiO$_2$ and Cu by nanoindentation. *Tribol. Lett.* 49, 85–94. doi: 10.1007/s11249-012-0050-5

Kim, N., Graham, S., and Hwang, K. J. (2014). Enhancement of the barrier performance in organic/inorganic multilayer thin-film structures by annealing of the parylene layer. *Mater. Res. Bull.* 58, 24–27. doi: 10.1016/j.materresbull.2014.03.022

Kirchheim, D., Wilski, S., Jaritz, M., Mitschker, F., Gebhard, M., Brochhagen, M., et al. (2017). Temperature-dependent transport mechanisms through PE-CVD coatings: comparison of oxygen and water vapor. *J. Phys. D Appl. Phys.* 50:395302. doi: 10.1088/1361-6463/aa80fd

Kovacik, J. (1999). Correlation between Young's modulus and porosity in porous materials. *J. Mater. Sci. Lett.* 18, 1007–1010. doi: 10.1023/A:1006669914946

Kumari, A., Yadav, S. K., and Yadav, S. C. (2010). Biodegradable polymeric nanoparticles based drug delivery systems. *Colloids Surf. B Biointerfaces* 75, 1–18. doi: 10.1016/j.colsurfb.2009.09.001

Lee, J. H., Kim, D. S., and Lee, Y. H. (2006). Room temperature deposition of silicon dioxide films by ion-assisted plasma enhanced chemical vapor deposition. *J. Electrochem. Soc.* 143, 1443–1451. doi: 10.1149/1.1836657

Lee, S., Shin, H. J., Yoon, S. M., Yi, D. K., Choi, J. Y., and Paik, U. (2008). Refractive index engineering of transparent ZrO$_2$-polydimethylsiloxane nanocomposites. *J. Mater. Chem.* 18, 1751–1755. doi: 10.1039/b715338d

Leterrier, Y. (2003). Durability of nanosized oxygen-barrier coatings on polymers. *Progress Mater. Sci.* 48, 1–55. doi: 10.1016/S0079-6425(02)00002-6

Liao, W. B., Chang, Y. C., Lin, Y. A., Chen, H. L., Chen, H. P., Wei, H. S., et al. (2018). SiO$_x$:C/SiO$_2$-like gas barrier multilayer thin films deposited by radio frequency magnetron sputtering-based plasma polymerization system. *Thin Solid Films* 660, 678–681. doi: 10.1016/j.tsf.2018.04.018

Lim, S. H., Seo, S. W., Jung, E., Chae, H., and Cho, S. M. (2016). Enhanced moisture barrier property and flexibility of zirconium oxide/polymer hybrid structures. *Korean J. Chem. Eng.* 33, 1070–1074. doi: 10.1007/s11814-015-0225-5

Liu, K.-C., Cheng, H.-L., Tsai, J.-R., Chiang, Y.-L., Hsieh, Y.-C., and Jan, D.-J. (2010). Investigation of SiO$_x$C$_y$ film as the encapsulation layer for full transparent OLED using hollow cathode discharge plasma at room temperature. *Thin Solid Films* 518, 6195–6198. doi: 10.1016/j.tsf.2010.01.052

Lu, S. K., Chen, S. C., Chen, T. H., Lai, L. W., Liao, R. M., and Liu, D. S. (2015). Barrier property and mechanical flexibility of stress controlled organosilicon/silicon oxide coatings on plastic substrates. *Surf. Coat. Technol.* 280, 92–99. doi: 10.1016/j.surfcoat.2015.08.063

Malitson, I. H. (2008). Interspecimen comparison of the refractive index of fused silica. *J. Opt. Soc. Am.* 55, 1205–1209. doi: 10.1364/JOSA.55.001205

Markov, D. A., Lillie, E. M., Garbett, S. P., and McCawley, L. J. (2014). Variation in diffusion of gases through PDMS due to plasma surface treatment and storage conditions. *Biomed. Microdevices* 16, 91–96. doi: 10.1007/s10544-013-9808-2

Matyka, M., Khalili, A., and Koza, Z. (2008). Tortuosity-porosity relation in porous media flow. *Phys. Rev. E Stat. Nonlinear Soft Matter Phys.* 78, 1–8. doi: 10.1103/PhysRevE.78.026306

Menčík, J. (2012) "Uncertainties and errors in nanoindentation," in *Nanoindentation in Materials Science*, ed J. Nemecek (London: IntechOpen), 67–68. doi: 10.5772/50002

Miyazaki, H. (2010). Refractive index and dielectric constant of SiO$_x$ films deposited by reactive sputtering. *Phys. Chem. Glasses Eur. J. Glass Sci. Technol. Part B* 51, 136−137.

Montero, I., Galan, L., De La Cal, E., Albella, J. M., and Pivin, J. C. (1990). Incorporation of OH radicals in anodic silicon oxide films studied by secondary ion mass spectroscopy, X-ray photoelectron spectroscopy and IR analysis. *Thin Solid Films* 193–194, 325–332. doi: 10.1016/S0040-6090(05)80042-2

Morra, M., Occhiello, E., Marola, R., Garbassi, F., Humphrey, P., and Johnson, D. (1990). On the aging of oxygen plasma-treated polydimethylsiloxane surfaces. *J. Colloid Interface Sci.* 137, 11–24. doi: 10.1016/0021-9797(90)90038-P

Moulder, J. F., Stickle, W. F., and Sobol, P. E. (2002). Poly(ethyl methacrylate) by XPS. *Surf. Sci. Spectra* 1, 346–350. doi: 10.1116/1.1247665

Nemani, S. K., Annavarapu, R. K., Mohammadian, B., Raiyan, A., Heil, J., Haque, M. A., et al. (2018). Surface modification of polymers: methods and applications. *Adv. Mater. Interfaces* 5, 1–26. doi: 10.1002/admi.201801247

Oliver, W. C., and Pharr, G. M. (1992). An improved technique for determining hardness and elastic modulus using load and displacement sensing indentation experiments. *J. Mater. Res.* 7, 1564–1583. doi: 10.1557/JMR.1992.1564

Pabst, W., Gregorova, E., and Ticha, G. (2006). Elasticity of porous ceramics — A critical study of modulus – porosity relations. *J. Eur. Ceram. Soc.* 26, 1085–1097. doi: 10.1016/j.jeurceramsoc.2005.01.041

Pan, P., Nesbit, L. A., Douse, R. W., and Gleason, R. T. (1985). The composition and properties of PECVD silicon oxide films. *J. Electrochem. Soc.* 132, 2012–2019. doi: 10.1149/1.2114272

Paparazzo, E., Fanfoni, M., Severini, E., and Priori, S. (2002). Evidence of SiOH species at the surface of aged silica. *J. Vac. Sci. Technol. A Vac. Surf. Films* 10, 2892–2896. doi: 10.1116/1.577726

Polyakov, B., Antsov, M., Vlassov, S., Dorogin, L. M., Vahtrus, M., Zabels, R., et al. (2014). Mechanical properties of sol–gel derived SiO$_2$ nanotubes. *Beilstein J. Nanotechnol.* 5, 1808–1814. doi: 10.3762/bjnano.5.191

Potscavage, W. J., Domercq, B., Graham, S., Kim, N., and Kippelen, B. (2009). A hybrid encapsulation method for organic electronics. *Appl. Phys. Lett.* 94:163308. doi: 10.1063/1.3115144

Reddy, I. N., Reddy, V. R., Sridhara, N., Rao, V. S., Mukhopadhyay, A. K., Sharma, A. K., et al. (2014). High emittance surface engineered metallic surfaces. *Ceram. Int.* 40, 14549–14554. doi: 10.1016/j.ceramint.2014.05.143

Rizzi, F., Qualtieri, A., Chambers, L. D., Megill, W. M., et al. (2013). Parylene conformal coating encapsulation as a method for advanced tuning of mechanical properties of an artificial hair cell. *Soft Matter* 9, 2584–2588. doi: 10.1039/c2sm27566j

Roberts, A. P., and Garboczi, E. J. (2000). Elastic properties of model porous ceramics. *J. Am. Ceram. Soc.* 83, 3041–3048. doi: 10.1111/j.1151-2916.2000.tb01680.x

Roberts, A. P., Henry, B. M., Sutton, A. P., Grovenor, C. R. M., Briggs, G. A. D., Miyamoto, T., et al. (2002). Gas permeation in silicon-oxide / polymer (SiO$_x$/PET) barrier films: role of the oxide lattice, nano-defects and macro-defects. *J. Membr. Sci.* 208, 75–88. doi: 10.1016/S0376-7388(02)00178-3

Schneider, J., Akbar, M. I., Dutroncy, J., Kiesler, D., Leins, M., Schulz, A., et al. (2009). Silicon oxide barrier coatings deposited on polymer materials for applications in food packaging industry. *Plasma Process. Polym.* 6, 700–704. doi: 10.1002/ppap.200931702

Shelekhin, A. B., Dixon, A. G., and Ma, Y. H. (1995). Theory of gas diffusion and permeation in inorganic molecular sieve membranes. *AIChE J.* 41, 58–67. doi: 10.1002/aic.690410107

Siracusa, V. (2012). Food packaging permeability behaviour: a report. *Int. J. Polym. Sci.* 2012:302029. doi: 10.1155/2012/302029

Sobrinho, A., Czeremuszkin, G., Latreche, M., and Wertheimer, M. R. (2000). Defect permeation correlation for ultrathin transparent barrier coatings on polymers. *J. Vac. Sci. Technol. A Vac. Surf. Films* 18, 149–157. doi: 10.1116/1.582156

Subhash, G., Hittepole, P., and Maiti, S. (2010). Mechanical properties of PECVD thin ceramic films. *J. Eur. Ceram. Soc.* 30, 689–697. doi: 10.1016/j.jeurceramsoc.2009.09.020

Tompkins, H. G., and Irene, E. A. (eds.). (2005). *Handbook of Ellipsometry*. Norwich, NY: William Andrew Publishing. doi: 10.1007/3-540-27488-X

Vasko, K., Noller, K., Mikula, M., Amberg-Schwab, S., and Weber, U. (2009). Multilayer coatings for flexible high-barrier materials. *Cent. Eur. J. Phys.* 7, 371–378. doi: 10.2478/s11534-009-0056-2

Vasquez, R. P., Maserjian, J., Madhukar, A., Lewis, B. F., Grunthaner, P. J., and Grunthaner, F. J. (2002). Local atomic and electronic structure of oxide/GaAs and SiO$_2$/Si interfaces using high resolution XPS. *J. Vac. Sci. Technol.* 16, 1443–1453. doi: 10.1116/1.570218

Vianna, C. E., da Silva, A. N. R., Morimoto, N. I., and Bonnaud, O. (2001). Analysis of SiO$_2$ thin films deposited by PECVD using an oxygen-TEOS-argon mixture. *Braz. J. Phys.* 31, 299–303. doi: 10.1590/S0103-97332001000200023

Webster, D. C., Patel, N. M., Hedrick, J. L., McGrath, J. E., and Dwight, D. W. (2005). Surface and bulk phase separation in block copolymers and their blends. Polysulfone/polysiloxane. *Macromolecules* 21, 2689–2696. doi: 10.1021/ma00187a007

Wuu, D. S., Chen, T. N., Wu, C. C., Chiang, C. C., Chen, Y. P., Horng, R. H., et al. (2006). Transparent barrier coatings for flexible organic light-emitting diode applications. *Chem. Vapor Depos.* 12, 220–224. doi: 10.1002/cvde.200506436

Yoshida, S., Hagiwara, K., Hasebe, T., and Hotta, A. (2013). Surface modification of polymers by plasma treatments for the enhancement of biocompatibility and controlled drug release. *Surf. Coat. Technol.* 233, 99–107. doi: 10.1016/j.surfcoat.2013.02.042

Yu, D., Yang, Y. Q., Chen, Z., Tao, Y., and Liu, Y. F. (2016). Recent progress on thin-film encapsulation technologies for organic electronic devices. *Opt. Commun.* 362, 43–49. doi: 10.1016/j.optcom.2015.08.021

Zeniieh, D., Ledernez, L., and Urban, G. (2014). Parylene-C as high performance encapsulation material for implantable sensors. *Proc. Eng.* 87, 1398–1401. doi: 10.1016/j.proeng.2014.11.704

Zhang, H., Ding, H., Wei, M., Li, C., Wei, B., and Zhang, J. (2015). Thin film encapsulation for organic light-emitting diodes using inorganic/organic hybrid layers by atomic layer deposition. *Nanoscale Res. Lett.* 10, 4–8. doi: 10.1186/s11671-015-0857-8

Ziarani, A. S., and Aguilera, R. (2012). Knudsen's permeability correction for tight porous media. *Transp. Porous Media* 91, 239–260. doi: 10.1007/s11242-011-9842-6